

PSFC/JA-00-29

**Two-Dimensional Full Wave Simulation of Microwave
Reflectrometry on Alcator C-Mod**

Y. Lin, J.H. Irby, R. Nazikian¹, E.S. Marmor

September 2000

Plasma Science and Fusion Center
Massachusetts Institute of Technology
Cambridge, MA 02139 USA

¹Princeton Plasma Physics Laboratory, Princeton, NJ 08543

This work was supported by the U.S. Department of Energy, Cooperative Grant No. DE-FC02-99ER54512. Reproduction, translation, publication, use and disposal, in whole or in part, by or for the United States government is permitted.

Submitted for publication to *Review of Scientific Instruments*.

Two-dimensional full wave simulation of microwave reflectometry on Alcator C-Mod

Y. Lin, J.H. Irby, R. Nazikian[†], E.S. Marmor, A. Mazurenko

MIT, Plasma Science and Fusion Center, Cambridge, MA 02139, USA

[†]Princeton Plasma Physics Laboratory, Princeton, NJ 08543, USA

Abstract

A new 2-D full-wave code has been developed to simulate ordinary (O) mode reflectometry signals caused by plasma density fluctuations. The code uses the finite-difference time-domain method with a perfectly-matched-layer absorption boundary to solve Maxwell's equations. Huygens wave sources are incorporated to generate Gaussian beams. The code has been used to simulate the reflectometer measurement of the quasi-coherent mode (60–250 kHz) associated with Enhanced D_α (EDA) H-modes in the Alcator C-Mod tokamak. It is found that an analysis of the realistic experimental layout is essential for the quantitative interpretation of the mode amplitude.

1 Introduction

The reflectometer in the Alcator C-Mod tokamak is an O-mode amplitude modulated (AM) reflectometer viewing along the mid-plane on the low field side of the magnetic axis [1] [2]. AM reflectometers use upper and lower sidebands around the carrier frequency, $f_0 \pm \Delta f$, to produce a differential signal for density profile measurement. Density profiles can be reconstructed from the measured group delays $d\phi/df \simeq [\phi(f + \Delta f) - \phi(f - \Delta f)]/2\Delta f$. The reflectometer has five channels at 50, 60, 75, 88, and 110 GHz. All these five channels can be used for density profile measurements. The 88 GHz channel of the reflectometer also measures the signal of each sideband independently for density fluctuations studies. Reflectometry has been invaluable in identifying the quasi-coherent density fluctuations (60 – 250 kHz in lab frame) associated with Enhanced D_α (EDA) H-modes (references [1] – [4]). Recent analysis has identified the quasi-coherent mode as responsible for much of the particle transport in the plasma edge.

Reflectometry is now a widely used tool for interpreting the behavior of plasma fluctuations. However, there is an incomplete understanding of the method and its limitations (for a recent review, see reference [5]). Various two-dimensional (2-D) models have been developed to interpret reflectometry

fluctuation measurements in recent years (see [6] – [12]). The cutoff density of the 88 GHz microwave channel ($n_c = 0.96 \times 10^{20} \text{ m}^{-3}$) is usually in the H-mode pedestal region, which has a sharp density gradient (density scale length $\leq 0.5 \text{ cm}$) and WKB approximation may fail. The quasi-coherent fluctuations have a poloidal wavelength $\lambda_\perp \simeq 1 \text{ cm}$ as measured by the phase contrast imaging (PCI) system. PCI measures line-integrated density fluctuations along 12 vertical chords. This wavelength corresponds to $\lambda_\perp/w_b \simeq 1$, where w_b is the incidence reflectometry microwave beam $1/e$ intensity half width. A model including the beam profile, plasma profile and curvature must be used to confidently interpret these reflectometer measurements.

A new code based on an earlier 2-D full-wave code (Maxwell code) [6] has been developed. The Maxwell code first demonstrated the importance of 2-D effects in interpreting reflectometry measurements. The new code incorporates additional electro-magnetic field computation techniques and is able to deal with Gaussian beam incidence and real plasma geometry.

We discuss the computation techniques used in the new 2-D full-wave code, and show simulations of the quasi-coherent fluctuations based on 2-D realistic geometry and an experimental density profile from an EDA H-mode. Simulation results are also compared with experimental observations.

2 Computation techniques

The 2-D full-wave code discussed in this paper has been developed based on an earlier code [6] to simulate O-mode ($\vec{E} = E_z(x, y)\vec{e}_z \parallel \vec{B}$) reflectometer fluctuation signals. We start from the normalized Maxwell's equations in the cold plasma approximation:

$$\frac{\partial H_x}{\partial t} = -\frac{\partial E_z}{\partial y} \quad (1)$$

$$\frac{\partial H_y}{\partial t} = \frac{\partial E_z}{\partial x} \quad (2)$$

$$\frac{\partial J_z}{\partial t} = \frac{n_e}{n_c}\pi E_z \quad (3)$$

$$\frac{\partial E_z}{\partial t} = -4\pi J_z + \frac{\partial H_y}{\partial x} - \frac{\partial H_x}{\partial y} \quad (4)$$

where, \vec{e}_y is the vertical (poloidal) direction and \vec{e}_x is the horizontal (radial) direction. Lengths are normalized to the vacuum wavelength of the incident beam, λ_0 ($\lambda_0 = 0.34$ cm for 88 GHz microwave), times are normalized to the microwave period, $\tau_0 = 1/f_0$. The critical density, n_c , is $(f_0/89.8)^2 \times 10^{20} \text{ m}^{-3}$ with f_0 in GHz.

The computation domain setup is illustrated in Figure 1. We use the standard finite-difference time-domain (FDTD) method as in [6] to calculate electric and magnetic fields. The grid size $\Delta x = \Delta y = 0.1\lambda_0$ and time step $\Delta t = 0.05\tau_0$ are used in order to obtain adequate precision and ensure computational stability.

Instead of a radiative boundary, as used in the Maxwell code, the new code uses a perfectly-matched-layer (PML) as the absorption boundary [13]. Numerical tests show that the constructed PML in our code has a reflection coefficient less than 0.1% for incidence angles up to 83° . Waves with near grazing incidence to one side of the boundary are actually absorbed in other sides of the PML. The PML ensures the reliability of long-time scale full-wave simulation.

We use the Huygens sources technique [14] to generate the incident Gaussian beam and also to separate reflected waves from the total fields in Maxwell's equations. A closed surface, Huygens surface, is constructed around the plasma (see Figure 1). By analytically calculating the incident fields, \vec{E}^{inc} and \vec{H}^{inc} , that would exist on the Huygens surface in the absence of plasma, we determine the Huygens source current densities on the surface, $\vec{M}^h = -\vec{n} \times \vec{E}^{inc}$ and $\vec{J}^h = \vec{n} \times \vec{H}^{inc}$, where \vec{n} is an inward unit vector normal to the surface. The fields inside the Huygens surface generated by \vec{M}^h and \vec{J}^h are total fields, but the fields outside the Huygens surface are the outgoing reflected waves only. In order to generate a Gaussian beam, we analytically calculate \vec{M}^h and \vec{J}^h using the beam waist radius ($1/e$ intensity radius) w_b , the distance from beam waist to plasma d and beam propagation angle θ_b , where $w_b \simeq 2.2\lambda_0$, $d \simeq 40\lambda_0$ and $\theta_b = -5^\circ$ relative to $+\vec{e}_x$ for the Alcator

C-Mod reflectometer. The Gaussian beam approximation is valid since the plasma is in the far field radiation region of the launch horn antenna.

The detected reflectometer signal is modelled as the integral of the complex E_z across the receiving horn aperture after passing through a horn directivity filter. For the Alcator C-Mod reflectometer, the receiving horn views at an angle of $+5^\circ$ relative to $+\vec{e}_x$. The horn is modelled with 24 dB gain, that is, the peak sensitivity is $10^{2.4}$ times that of a 4π solid angle average.

The plasma is assumed to be static for each run of the simulation, and the simulation time is long enough so that steady state is reached. The reflectometer responses are the combination of many runs with identical initial beam conditions but different plasma fluctuation phases.

3 Simulation of Alcator C-Mod reflectometer:

The simulation has been performed based on the Alcator C-Mod reflectometer geometry and experimental density profile to study the measurement of the quasi-coherent density fluctuations in the EDA H-mode.

3.1 Simulation parameters

Figure 2 shows a typical EDA H-mode discharge. The D_α enhancement starts at $t \simeq 0.70$ s shortly after the L-H transition at $t \simeq 0.69$ s. We use a *tanh*

fit for the experimental density profile derived from a high spatial resolution visible continuum array [15] (Figure 3):

$$n_0(x, y = 0) = 0.8n_c \left[1 + 0.025x/\lambda_0 + \tanh \left(\frac{x - 10\lambda_0}{2\lambda_0} \right) \right] \quad (5)$$

where, $x = 0$ is the model plasma edge at the mid-plane ($y = 0$), and the critical density $n_c = 0.96 \times 10^{20} \text{ cm}^{-3}$ for 88 GHz microwave. We use a circularly shaped density profile with the center at $X_P = 45\lambda_0$. The radius of curvature, X_P , is estimated from EFIT reconstructed flux surfaces.

A poloidal fluctuation with $\lambda_\perp = 4\lambda_0$ is introduced to model the quasi-coherent density fluctuations:

$$\tilde{n}_{coh}(x, y)/n_0 = \eta \times \exp \left[-(x - 9.5\lambda_0)^2 \right] \cos(2\pi y/\lambda_\perp + \phi_f) \quad (6)$$

where, η is referred to as the quasi-coherent fluctuation level \tilde{n}/n and ϕ_f is the fluctuations phase. The actual form also includes the plasma curvature. The fluctuation radial shape for $x > x_c \simeq 10\lambda_0$ is unimportant due to insignificant microwaves penetration.

3.2 Simulation results

Figure 4 shows part of the computation domain with E_z contours and the density critical layer for the realistic geometry simulation. The computation domain is $-17\lambda_0 < y < 17\lambda_0$ and $-42\lambda_0 < x < 16\lambda_0$. The left Huygens

surface is at $x = -\lambda_0$. The E_z field at $x > -\lambda_0$ is the total field of the incident beam and the reflected waves while only reflected waves are propagating to the left at $x < -\lambda_0$. Interference patterns between the incident Gaussian beam and reflected waves are clear for $x > -\lambda_0$.

Figure 5 shows the phase response versus fluctuation level for three different cases. $\Delta\phi = \phi_{max} - \phi_{min}$ is the reflectometer phase response in one period of the quasi-coherent mode. In the case of the 2-D full wave simulation with plasma curvature, there is a nearly linear relation between $\Delta\phi$ and η for $\eta \leq 0.1$. The 2-D full wave result without plasma curvature (slab geometry) and a 1-D numerical calculation based on geometric optics are also shown. The slab geometry result is smaller than that with curvature. The result with plasma curvature is closer to the 1-D geometric optics calculation.

For real geometry, there is a limit of the mode amplitude that can be measured by reflectometry. Asymmetry in the measured spectrum introduces ellipticity in the complex plane of the reflectometer signals (Figure 6). As the mode amplitude increases, the point $(0,0)$ may be enclosed by the curve and the phase changes 2π for a fluctuations period, which leads to the phase runaway phenomenon [10] [12] [16]. For our simulation parameters, phase runaway occurs at $0.125 < \eta < 0.15$ as shown in Figure 6. For even higher fluctuations the linearity between the reflectometer phase and fluctua-

tion level breaks down due to large variations in the phase across the receiving horn aperture even when no phase runaway exists. Figure 7 shows the phase difference across the horn aperture for two fluctuation phases $\phi_f = 0$ and π for different fluctuation levels η . For low fluctuation level, the phase difference is nearly constant across the aperture. For high fluctuation levels, the variation is large due to strong scattering. The reflectometer signal, which is the integral of the E_z field at the horn aperture after filtering by the horn directivity function, no longer linearly represents the fluctuation level.

4 Experimental observations

A plot of the reflectometer phase response to the quasi-coherent mode in EDA plasma versus PCI measured mode amplitude is shown in Figure 8. These data are taken from $0.8 < t < 1.0$ s for the discharge shown in Figure 2. PCI signals are line-integrated density fluctuations. Figure 8 shows a linear relation between the quasi-coherent fluctuation levels in the reflectometer data and the PCI signals. The fluctuations levels are the integrated auto-spectral densities around the coherent peak frequency, which occurs at ~ 100 kHz in this time period. The auto-spectral densities are calculated in a 2 ms time window. We infer the fluctuations level in Figure 8 to be $0.025 \leq \eta \leq 0.05$ based on the simulation result for 2-D geometry with plasma curvature (Fig-

ure 5). It is comparable to the level $\tilde{n}/n \sim 0.02 - 0.04$ estimated from PCI measurement based on an assumed mode radial width $\Delta r \simeq 1$ cm.

5 Conclusion

A new 2-D full-wave code has been developed to simulate O-mode reflectometry with realistic geometry. The reflectometer measurement of the quasi-coherent mode associated with the EDA H-mode has been studied using the code based on Alcator C-Mod reflectometer parameters and a typical plasma profile. At low fluctuation amplitudes, the reflectometer phase can correctly represent the coherent fluctuation level. Phase runaway is observed at some fluctuation levels. The linearity between reflectometer phase and fluctuation level breaks down at high fluctuation amplitudes. The role of curvature and receiving system geometry is shown to be critical for the quantitative interpretation of reflectometry measurements, and leads to a result in broad agreement with 1-D geometric optics for the EDA quasi-coherent mode at low fluctuation levels.

Acknowledgements

The work is supported by US-DOE D.o.E. Coop. Agreement DE-FC02-99ER54512 and DE-AC02-76-CHO-3073.

References

- [1] Y. Lin, J. Irby, P. Stek, I. Hutchinson, J. Snipes, R. Nazikian, M. McCarthy, Rev. Sci. Instrum. **70** (1), 1078-1081 (1999).
- [2] P.C. Stek, PhD dissertation, *Reflectometry Measurements on Alcator C-Mod*, Massachusetts Institute of Technology, March, 1997.
- [3] M. Greenwald, *et al*, Phys. Plasmas **6** (5), 1943-1949 (1999).
- [4] M. Greenwald, *et al*, Plasma Phys. Control. Fusion **42**, A263-A269 (2000).
- [5] E. Mazzucato, Rev. Sci. Instrum. **69** (6), 2201-2217 (1998).
- [6] J.H. Irby, S. Horne, I.H. Hutchinson, P.C. Stek, Plasma Phys. Control. Fusion **35**, 601-618 (1993).
- [7] R. Nazikian and E. Mazzucato, Rev. Sci. Instrum. **66** (1), 392-398 (1995).
- [8] E. Mazzucato and R. Nazikian, Physical Review Letters, Vol. 71, No. 12, 1840-1843, 1993.
- [9] E. Mazzucato, Rev. Sci. Instrum. **69** (4), 1691-1698 (1998).
- [10] G.D. Conway, Plasma Phys. Control. Fusion **41**, 65-92 (1999).
- [11] V. Zhuravlev, J. Sanchez and E. de la Luna, Plasma Phys. Control. Fusion **38**, 2231-2242 (1996).

- [12] E. Holzhauser, M. Hirsch, T. Grossmann, B. Brañas and F. Serra, Plasma Phys. Control. Fusion **40**, 1869-1886 (1998).
- [13] J. Berenger, J. of Computational Physics **114**, 185-200 (1994).
- [14] R. Holland and J.W. Williams, IEEE Transactions on Nuclear Science, Vol. NS-30, No. 6, 4583-4588, December, 1983.
- [15] E.S. Marmor, *et al*, this conference.
- [16] A. Ejiri, K. Shinohara and K. Kawahata, Plasma Phys. Control. Fusion **39**, 1963-1980 (1997).

Captions

Figure 1: The computation domain. The incident Gaussian beam is generated by sources on the Huygens surface. A perfect-matched-layer (PML) is constructed as the absorption boundary. Outgoing waves near the receiving plane filtered by a 2-D horn directivity function are used to model the reflectometer measurement.

Figure 2: An Enhanced D_α H-mode discharge with 2 MW of ICRF heating and 800 kA of plasma current. The plasma is in H-mode at $0.69 \leq t \leq 1.15$ s. The D_α enhancement starts at $t \simeq 0.70$ s shortly after the L-H transition.

Figure 3: The n_e profile derived from a high resolution visible continuum array at $t = 0.820$ s of the discharge in Figure 2. The x -axis is shifted so that $n(x = 0) = 0$ for the *tanh* fit curve. The critical density $n_c = 0.96 \times 10^{20} \text{ m}^{-3}$. The last closed flux surface (LCFS) is also shown.

Figure 4: Electrical field E_z contours at part of the computation domain ($-17\lambda_0 < y < 17\lambda_0$ and $-42\lambda_0 < x < 16\lambda_0$). The critical layers are also drawn with broken lines. E_z contours are drawn at $\frac{1}{4}E_0$, $\frac{1}{2}E_0$ and E_0 , where E_0 is the maximal incident E_z . The Huygens surface is at $x = -\lambda_0$. No fluctuations in figure (a), while $\eta = 0.025$ in figure (b).

Figure 5: Modelled reflectometer phase responses versus fluctuation level. $\Delta\phi = \phi_{max} - \phi_{min}$ is the reflectometer phase response over one period of the quasi-coherent mode. The results without plasma curvature (slab) and a 1-D numerical calculation are also shown.

Figure 6: Modelled reflectometer signal for one fluctuation period in complex plane. A_0 is the incidence beam amplitude. Phase runaway occurs at $0.125 < \eta < 0.15$ when point $(0,0)$ is enclosed by the curve. The linearity between $\Delta\phi$ and η is broken for higher fluctuation levels.

Figure 7: The phase difference across the receiving horn aperture between signals with $\phi_f = 0$ and π . y_{horn} is the horn aperture center. For low fluctuation levels, the phase difference is nearly constant in the entire aperture. For high fluctuation levels, the variation is large.

Figure 8: Comparison of quasi-coherent fluctuations levels measured by the reflectometer versus PCI ($0.8 < t < 1.0$ s for the discharge in Figure 2). Data are taken from time windows with low turbulence levels. A linear fit is also shown. The fluctuations levels are integrated auto-spectral densities around the quasi-coherent mode peak (~ 100 kHz in this period).

Figures:

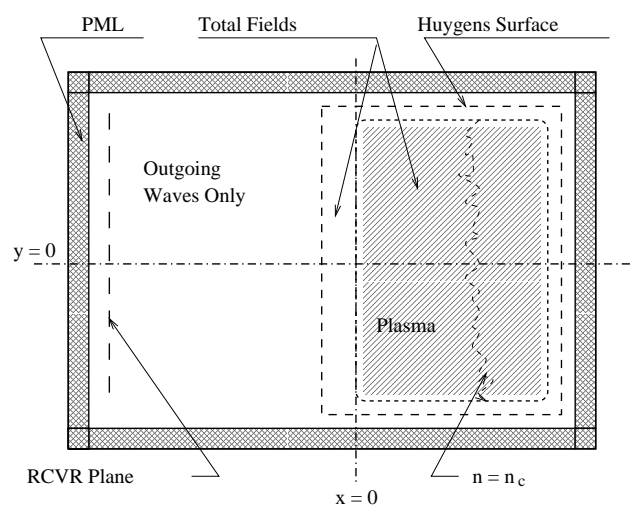


Figure 1: (Y. Lin)

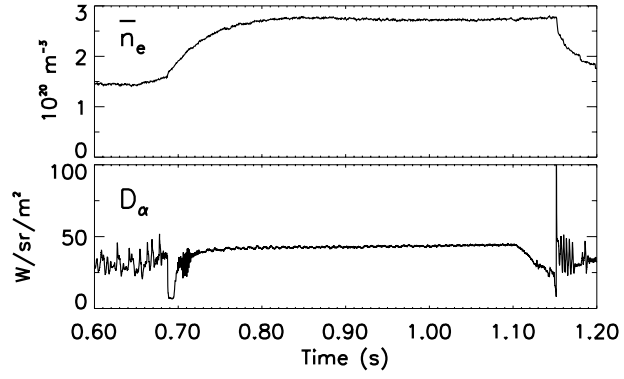


Figure 2: (Y. Lin)

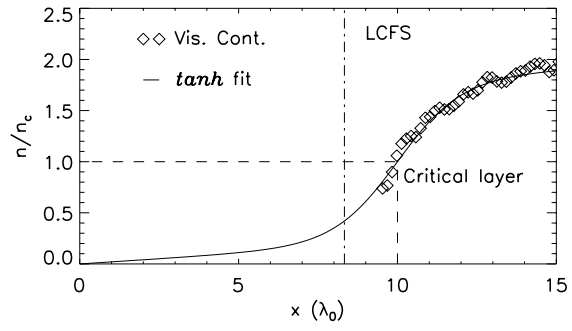


Figure 3: (Y. Lin)

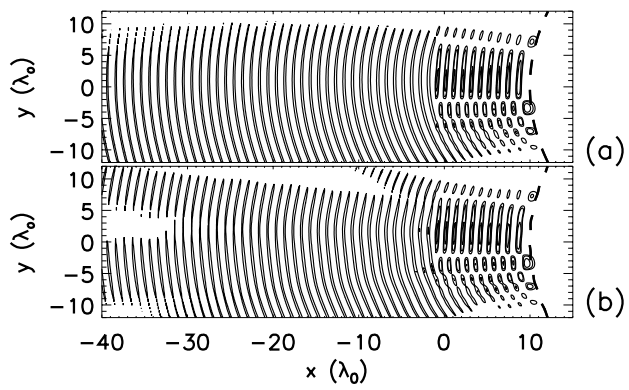


Figure 4: (Y. Lin)

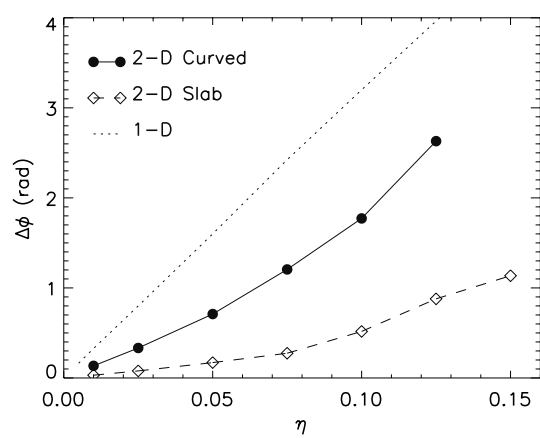


Figure 5: (Y. Lin)

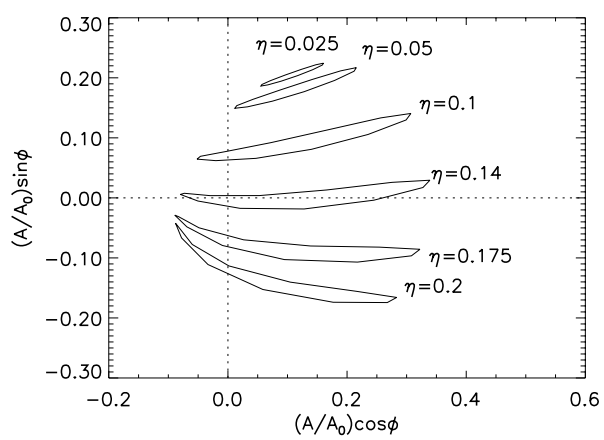


Figure 6: (Y. Lin)

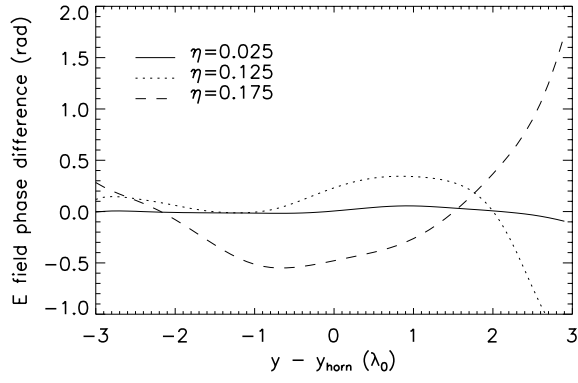


Figure 7: (Y. Lin)

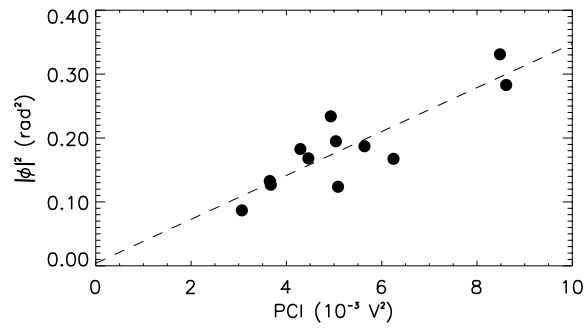


Figure 8: (Y. Lin)